Supplementary Information For "Mechanical coupling between myosin molecules causes differences between ensemble and single molecule measurements"

Sam Walcott*, David M. Warshaw† and Edward P. Debold‡

*Department of Mathematics, University of California at Davis

†Molecular Physiology and Biophysics, University of Vermont

‡Department of Kinesiology, University of Massachusetts at Amherst

June 6, 2012

Mathematical implementation of the model

We consider the 4-state model for actomyosin interaction shown in Fig. 1 of the main text and reproduced here below (see Fig. 1). Briefly, unbound (or weakly-bound) myosin with ADP and phosphate (P_i) in its active site transitions to a state where it strongly binds to actin. We label the former state (un-/weakly-bound with ADP and P_i in the active site) state 1, while the latter state (bound with ADP in the active site) is state 2. Once strongly bound, myosin may release ADP in a force-dependent process. It then enters the rigor state, state 3. Having released both ADP and phosphate, myosin's nucleotide binding pocket is empty and the molecule may bind ATP, and upon doing so, unbind from actin. This unbound state with ATP in the active site is state 4. Once ATP is bound and myosin has detached from actin, myosin may hydrolyze ATP and revert to the pre-powerstroke conformation, state 1 (see Fig. 1).

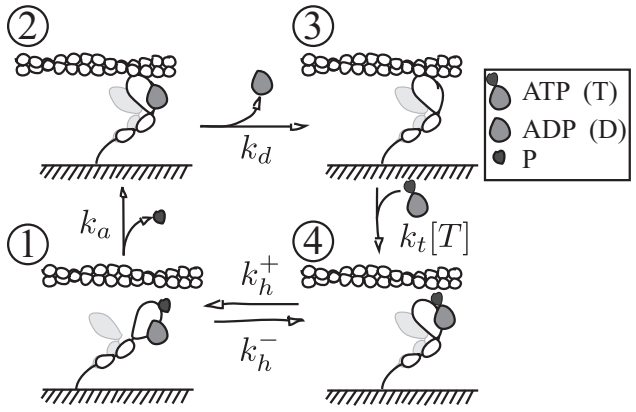

Figure 1: The kinetic scheme of myosin's interaction with actin. See Fig. 1 of the main text for a more detailed description.

In the model, some care must be given to determining which states and state transitions depend on molecular extension. In particular, the probability of a myosin molecule being in a state where myosin is unbound from actin (states 1 and 4) is a function of time only $n(t)$. However, when myosin is attached to actin (states 2 and 3), we must consider the probability density of myosin being in that state with some extension x, $\eta(x,t)$. The probability that myosin is in this attached state is then $N(t) = \int_{-\infty}^{\infty} \eta(x,t)dx$. Therefore, $\eta(x,t)$ has units of 1/length, while $n(t)$ and $N(t)$ are dimensionless.

State transitions, too, depend on molecular extension (e.g. ADP release occurs at a rate $k_d(x)$). Furthermore, when myosin binds to actin we must consider not only the probability of myosin binding, but also the probability density of myosin binding with some extension x. This rate density is $\kappa_a(x)$ and the overall attachment rate is $k_a = \int_{-\infty}^{\infty} \kappa_a(x)dx$. The rate density has units of 1/length $\cdot$ time.

Assuming a large number of cross-bridges, so that the mean-field approximation is appropriate, and assuming that myosin may bind anywhere on actin (a dense binding site approximation [41]) the system is then governed by the following coupled integro-PDEs [e.g. 20, 29, 30]:

$$\begin{aligned}
\frac{\partial \eta_2}{\partial t} + v\frac{\partial \eta_2}{\partial x} &= \kappa_a(x)n_1 - k_d(x)\eta_2 \\
\frac{\partial \eta_3}{\partial t} + v\frac{\partial \eta_3}{\partial x} &= k_d(x)\eta_2 - k_T[T]\eta_3 \\
\frac{dn_4}{dt} &= \int_{-\infty}^{\infty} k_T[T]\eta_3 dx + n_1 k_h^- - n_4 k_h^+ \\
\frac{dn_1}{dt} &= -\left(\int_{-\infty}^{\infty} \kappa_a(x)dx + k_h^-\right) n_1 + n_4 k_h^+
\end{aligned} \tag{1}$$

where $n_i(t)$ is probability, $\eta_i(x,t)$ a probability density, k_i a rate constant and $\kappa_i(x)$ a rate density. Mass conservation gives us the following expression (which is implicit in the above four equations):

$$n_1 + n_4 + \int_{-\infty}^{\infty} \eta_2 dx + \int_{-\infty}^{\infty} \eta_3 dx = 1$$

Note that we assume k_T is insensitive to myosin extension [24]. Reactions that occur while myosin is unbound from actin (k_h^+ and k_h^-) occur at a constant rate. We are then left with specifying functions for $\kappa_a(x)$, the attachment rate density, and $k_d(x)$ the ADP release rate.

Experimental measurements suggest that ADP release occurs with the following force dependence [3, 49, 24]:

$$k_d(x) = k_d^0 \exp(-F\delta_x/k_BT) = k_d^0 \exp(k(x+d)\delta_x/k_BT)$$

where we have assumed that myosin acts as a linear spring of stiffness k (note that this molecular stiffness should not be confused with the rate constants, which are given by k_i where $i = h, d, T, \cdots$).

Assuming that binding sites are dense along actin, and assuming that myosin binds equally at these binding sites, we might expect that myosin's binding density as a function of extension should be roughly proportional to the probability that free myosin has a given extension. Myosin then has a binding density of the form

$$\kappa_a(x) = k_a\sqrt{\frac{k}{2\pi k_BT}} \exp\left(-\frac{kx^2}{2k_BT}\right) \tag{2}$$

Such Gaussian attachment rate densities are common in models of acto-myosin interaction [36, 13, 44].

A more careful derivation of this rate density [41, 51], is

$$\kappa_a(x) = \kappa_0 \exp\left(-\frac{kx^2}{2k_BT} + \frac{kw}{k_BT}(\sqrt{L^2+x^2} - L)\right) = \kappa_0 \exp\left(-\frac{kx^2}{2k_BT}\left[1 - \frac{wL}{2x^2}(\sqrt{1+(x/L)^2} - 1)\right]\right)$$

where κ_0 is the reaction rate density at $x = 0$, w is the width of the potential well associated with the binding site and L is the minimum separation distance between actin and unstrained myosin. The Gaussian approximation, Eq. 2, may be seen as simply the assumption that w is small. Typical values of myosin extension x are expected to be on the order of tens of nanometers. Actomyosin separation L and the binding site width are presumably an order of magnitude smaller than this, so that it seems reasonable to assume $wL/x^2 \ll 1$. Given these assumptions, we can solve the integro-PDEs numerically [51]. It is useful to also consider approximations to the steady-state solution of these equations.

A semi-analytic approximation

We now derive a semi-analytic approximation to the solution of these equations in steady-state. In particular, besides solving for $\eta_2(x)$ as a function of actin sliding rate v, we also solve for ensemble force F as a function

of sliding rate v. These solutions include the exponential integral function $E_1(x) = \int_1^\infty \exp(-xt)dt/t$ and the integral $Q(x) = \int_0^\infty t\exp(-x\exp(t))dt$. These values are tabulated. To find this solution, we make two additional assumptions:

1. We assume that the ATP concentration, $[T]$, is large so that the state $\eta_3 \approx 0$;
2. We assume that the attachment rate density can be approximated by a delta function $\kappa_a \approx k_a^0\delta(x)$.

With these assumptions, the equations reduce to (where we use the conservation of mass rather than the equation for n_1)

$$\begin{aligned} v\frac{d\eta_2}{dx} &= k_a^0\delta(x)n_1 - k_D\exp(kx\delta_x/k_BT)\eta_2 & (3)\\ 0 &= -(k_a^0 + k_h^-)n_1 + n_4k_h^+ & (4)\\ 1 &= n_4 + n_1 + \int_{-\infty}^{\infty}\eta_2 dx & (5)\end{aligned}$$

where $k_D = k_d^0\exp(kd\delta_x/k_BT)$. We may further simplify these equations by introducing the symbol $N = \int_{-\infty}^{\infty}\eta_2 dx$, and solving for η_2, which we now denote simply by ρ. Then, we have a single integro-differential equation:

$$v\frac{d\rho}{dx} = \frac{k_h^+k_a^0}{k_a^0 + k_h^- + k_h^+}(1-N)\delta(x) - k_D\exp(kx\delta_x/k_BT)\rho$$

near zero, we may write

$$\rho(0^+) - \rho(0^-) = \frac{k_h^+k_a^0}{v(k_a^0 + k_h^- + k_h^+)}(1-N)$$

since $\rho(0^+) = 0$, this equation gives an expression for ρ in the neighborhood of zero, which we henceforth call $\rho(0)$ as

$$\rho(0) = -\frac{k_h^+k_a^0}{v(k_a^0 + k_h^- + k_h^+)}(1-N)$$

away from zero, we may write

$$\rho(x) = \rho(0)\exp\left(-\frac{k_Dk_BT}{vk\delta_x}\left(\exp(kx\delta_x/k_BT) - 1\right)\right)$$

combining the two expressions, we may explicitly write out the steady-state distribution $\rho(x)$ as

$$\rho(x) = -\frac{k_h^+k_a^0}{v(k_a^0 + k_h^- + k_h^+)}(1-N)\exp\left(-\frac{k_Dk_BT}{vk\delta_x}\left(\exp(kx\delta_x/k_BT) - 1\right)\right)$$

with the assumption that $x \le 0$. We must now solve for N by integrating both sides with respect to x:

$$N = \frac{k_h^+k_a^0k_BT\exp\left(\frac{k_Dk_BT}{vk\delta_x}\right)E_1\left(\frac{k_Dk_BT}{vk\delta_x}\right)}{vk\delta_x(k_a^0 + k_h^- + k_h^+) + k_h^+k_a^0k_BT\exp\left(\frac{k_Dk_BT}{vk\delta_x}\right)E_1\left(\frac{k_Dk_BT}{vk\delta_x}\right)}$$

so that, finally, we have

$$\rho(x) = -\left(\frac{k\delta_xk_h^+k_a^0\exp\left(\frac{k_Dk_BT}{vk\delta_x}\right)}{vk\delta_x(k_a^0 + k_h^- + k_h^+) + k_h^+k_a^0k_BT\exp\left(\frac{k_Dk_BT}{vk\delta_x}\right)E_1\left(\frac{k_Dk_BT}{vk\delta_x}\right)}\right)\exp\left(-\frac{k_Dk_BT}{vk\delta_x}\exp(kx\delta_x/k_BT)\right)$$

we are most interested in force, which can be determined from the expression

$$F = \int_{-\infty}^{0} k(x+d)\rho(x)dx$$

which gives

$$F = \left(\frac{dkk_BTk_h^+k_a^0 \exp\left(\frac{k_Dk_BT}{vk\delta_x}\right)}{vk\delta_x(k_a^0 + k_h^- + k_h^+) + k_h^+k_a^0k_BT\exp\left(\frac{k_Dk_BT}{vk\delta_x}\right)E_1\left(\frac{k_Dk_BT}{vk\delta_x}\right)} \right) \left[\frac{k_BT}{dk\delta_x} Q\left(\frac{k_Dk_BT}{vk\delta_x}\right) + E_1\left(\frac{k_Dk_BT}{vk\delta_x}\right) \right] \tag{6}$$

This is the expression of steady-state force as a function of velocity (i.e. the force-velocity curve).

An analytic approximation in the absence of external force

Several experiments of interest, most notably the *in vitro* motility assay, involve myosin moving actin in the absence of external force. We will first non-dimensionalize Eq. 6 and then consider the solution for $F = 0$. We will find a simple approximation of its value. Next, we will derive expressions for two values of interest, d_∞ the distance over which myosin stays attached to actin and t_∞ the strong binding lifetime. Again, simple analytic approximations for these variables can be found. We discuss the relationship between these variables and the value of these variables in single molecule experiments.

It is convenient to introduce a series of non-dimensional variables: $\mathcal{V} = -v/dk_d^0$, $E = -dk\delta_x/k_BT$, $V = \mathcal{V}E\exp(E)$, $K = k_D(k_a^0 + k_h^- + k_h^+)/k_h^+k_a^0$, $\mathcal{F} = F/d \cdot k$ so that

$$\mathcal{F} = \left(\frac{1}{VK\exp(-1/V) + E_1(1/V)} \right) \left[-\frac{1}{E} Q(1/V) + E_1(1/V) \right]$$

when $\mathcal{F} = 0$, this equation reduces to

$$E_1(1/V) - \frac{1}{E} Q(1/V) = 0 \tag{7}$$

This equation is the solution of Eq. 6 for $F = 0$. It is transcendental, but can be numerically evaluated. Note that the value of V, the non-dimensional speed, and also $\mathcal{V}$ a variable we will discuss in detail below, depend only on the non-dimensional parameter E.

If E is relatively large (and thus V is large) there is an analytic approximation of this unloaded contraction speed.

$$-\gamma + \ln(V) = \frac{1}{E}\left(\frac{\pi^2}{12} + \frac{\gamma^2}{2} - \gamma\ln(V) + \frac{(\ln(V))^2}{2} \right)$$

so that

$$V \approx \exp\left(\gamma + E \pm \sqrt{E^2 - \frac{\pi^2}{6}} \right)$$

or since $V = E\mathcal{V}\exp(E)$,

$$\mathcal{V} \approx \frac{1}{E}\exp\left(\gamma + E\sqrt{1 - \left(\frac{\pi}{E}\right)^2 \frac{1}{6}} \right) \tag{8}$$

Recall that $\mathcal{V} = v/k_d^0 d$. The variable dk_d^0 can also be written d_1/t_1, where t_1 is myosin's strong binding lifetime and d_1 myosin's unitary step size as measured in the laser trap at high $[ATP]$. This expression can be thought of as the rate at which a single myosin molecule moves actin, v_1. Ignoring intermolecular interactions, this is the rate a large ensemble of myosin molecules would move actin [e.g. 47, 54]. Thus, $\mathcal{V}$ is the ratio of actin speed with intermolecular interactions (v) to actin speed without intermolecular interactions (v_1). In general, Eq. 8 shows that $v \neq v_1$, and in particular $v > v_1$ (see Fig. 5 of the main text) – in other words, intermolecular interactions accelerate free actin speed.

Assuming that actin speed is limited by ADP release (sometimes called the "detachment limited" model for actin motility [21, 40]), then actin speed can be written $v = d_\infty/t_\infty$. The result $v > v_1$ then means that $d_\infty > d_1$ and/or $t_\infty < t_1$. We now show that both of these inequalities are correct: intermolecular interactions increase the distance over which myosin remains bound to actin d_∞ while decreasing the time that myosin remains bound to actin t_∞.

Attachment time and distance

The attachment distance d_∞ is the average distance that actin moves during a single myosin attachment. For a single, isolated molecule, myosin binds at $x \approx 0$ and undergoes its power stroke of size d. Actin rapidly slides forward a distance d and myosin relaxes to an un-extended configuration. Thus, in the single molecule case, $d_1 = d$ since actin travels a distance d each time myosin attaches to actin.

To calculate d_∞ from the simplified model described in the previous subsection, we must find the average extension of the detaching myosin molecules. Since they bind in the unextended position, $x = 0$, d_∞ is equal to the expectation value of the extension of detaching molecules. This can be written

$$d_\infty = \langle x \rangle_{detach} = \frac{\int_{-\infty}^{\infty} k_d(x)\rho(x)x dx}{\int_{-\infty}^{\infty} k_d(x)\rho(x)dx}$$

using the expressions derived in the previous section, we have

$$d_\infty = \frac{\int_{-\infty}^{0} \exp(kx\delta_x/k_BT) \exp\left(-\frac{k_D k_B T}{vk\delta_x} \exp(kx\delta_x/k_BT)\right) x dx}{\int_{-\infty}^{0} \exp(kx\delta_x/k_BT) \exp\left(-\frac{k_D k_B T}{vk\delta_x} \exp(kx\delta_x/k_BT)\right) dx}$$

which can be solved and non-dimensionalized (where we introduce the non-dimensional variable $\mathcal{D} = d_\infty/d$):

$$\mathcal{D} = \frac{1}{E} \exp\left(\frac{1}{V}\right) E_1\left(\frac{1}{V}\right) \tag{9}$$

Which, when combined with Eq. 7, provides a good approximation of attachment distance (see Fig. 5 of the main text). Note that, like Eq. 7, this expression depends only on the non-dimensional variable E.

Again, if E (and therefore V) is relatively large, we may make a simple approximation:

$$\mathcal{D} \approx 1 + \sqrt{1 - \frac{\pi^2}{6E^2}} \tag{10}$$

Here, it is clear that $\mathcal{D} > 1$, so that the attachment distance is always larger than d and thus intermolecular interactions increase the attachment distance. Note that there is an upper bound on d_∞ of $2d$.

The attachment lifetime, t_{on}, is the average time that myosin stays strongly bound to actin.

$$t_\infty = \langle t \rangle_{detach} = \frac{\int_{-\infty}^{\infty} k_d(x)\rho(x)t_a dx}{\int_{-\infty}^{\infty} k_d(x)\rho(x)dx}$$

where t_a is the time since a myosin molecule at x has been attached. Note that our assumption of δ-function attachment rate density allows us to write the relation $t_a = x/v$. Thus, we have

$$t_\infty = \langle t \rangle_{detach} = \frac{1}{v} \frac{\int_{-\infty}^{\infty} k_d(x)\rho(x)x dx}{\int_{-\infty}^{\infty} k_d(x)\rho(x)dx} = \frac{d_\infty}{v}$$

This result is not surprising, but demonstrates that actin motility is indeed detachment limited, since we may write

$$v = \frac{d_\infty}{t_\infty}$$

Recall that here we consider large $[ATP]$, so the non-dimensional variable of interest is $\mathcal{T} = t_\infty/t_1 = t_\infty k_d^0$, so that we may non-dimensionalize to find

$$\mathcal{V} = \frac{\mathcal{D}}{\mathcal{T}} \tag{11}$$

This equation allows us to find $\mathcal{T}$ from Eq. 7 and 9. Note that, since both $\mathcal{V}$ and $\mathcal{D}$ depend only on the parameter E, so too does $\mathcal{T}$.

As before, if E (and therefore V) is relatively large, we may make a simple approximation

$$\mathcal{T} \approx E\left(1 + \sqrt{1 - \frac{1}{6}\left(\frac{\pi}{E}\right)^2}\right) \exp\left(-\gamma - E\sqrt{1 - \frac{1}{6}\left(\frac{\pi}{E}\right)^2}\right) \tag{12}$$

Validation

Using estimates of the eight parameters (k_a, k_d^0, k_h^+, k_h^-, k_T, k, δ_x and d) for both smooth and skeletal myosin, we find that $E \approx 1.88$ and $E \approx 1.35$, respectively, apply to smooth and to skeletal myosin *in vitro*. We performed Monte-Carlo free motility simulations of large myosin ensembles (400 available heads) at these values, and then varied myosin stiffness k to determine the validity of the analytic and semi-analytic approximations. For smooth muscle myosin, we considered $[ATP] = 1$mM and 4mM. For skeletal muscle myosin, we considered $[ATP] = 4$mM. At these high ATP concentrations, rigor myosin should contribute negligibly to force, as assumed in our derivation of the approximations.

As shown in Fig. 5 of the main text, the semi-analytic approximation agrees with the simulations for all values of E considered ($E = 0.899, 1.348, 1.570, 1.797, 1.884, 2.198, 2.512$ and 2.826). The analytic approximation, valid at large E, provide reasonable estimates of $\mathcal{V}$ and $\mathcal{T}$ for all but the smallest value of E ($E = 0.899$), but only provide good estimates of $\mathcal{D}$ for larger values of E ($E = 1.797, 1.884, 2.198, 2.512$ and 2.826). Based on these results, we conclude that the analytic approximation for large E (Eq. 8) applies to smooth muscle myosin, while the semi-analytic approximation must be applied to skeletal muscle myosin.

Estimating parameters

Our kinetic model has eight parameters, k_h^+, k_h^-, k_t, k_d^0, k_a, δ_x, k and d. For smooth muscle, we may estimate all model parameters except myosin's stiffness k from the literature. For skeletal muscle, we do not know k, δ_x and k_d^0. Ideally, we would determine these unknown values from fits to all available data, however such an approach is intractable as simulations are too computationally expensive. Instead, our approach was to find the parameter values that best fit a subset of the data, and then to test whether simulations with these parameter values fit the remainder of the data. We now describe our parameter estimates from literature and then our fitting procedure.

Parameter estimates from literature

We consider experiments with both skeletal muscle myosin (chicken pectoralis) and smooth muscle myosin (plus insert). Temperature varied slightly in the experiments, with laser trap experiments conducted approximately at room temp [e.g. 53, 15, 11], and motility experiments conducted approximately at 30 C [e.g. 12, 16]. Experiments were performed in buffers with an ionic strength of approximately 0.025 M [e.g. 53, 15, 11, 12, 16]. In this section, we describe the parameter estimates from previous direct experimental measurements; in the next section, we describe our indirect parameter estimates.

For smooth muscle simulations, we use the laser trap measurements of Kad et al. [24], of $k_d^0 = 18\text{s}^{-1}$ and $\delta_x = -2.6$nm. These values agree with solution measurements of ADP release that range from 15 to 79s^{-1} [31, 8, 42, 24], and the measurements of Veigel et al. [49] of $\delta_x = -2.7$nm. Based on solution measurements of the pseudo first-order rate of ATP binding and myosin detachment from actin of $k_T = 1$ to $2\mu\text{M}^{-1}\text{s}^{-1}$ [31, 24], we used $k_T = 1.2\mu\text{M}^{-1}\text{s}^{-1}$. We assume that ATP hydrolysis off actin occurs at $k_h^+ = 100\text{s}^{-1}$ [39] and the reaction reverses at $k_h^- = 10\text{s}^{-1}$ [19]. Using these estimates of rate constants, the overall attachment rate k_a, including phosphate release and a transition from a weakly- to a strongly-bound state, may be estimated from steady-state ATP turnover experiments (briefly, we used the kinetic model in Fig. 1 and, since these experiments are performed with myosin free in solution, we used the values of all rate constants in the absence of force. Instead of the set of linear integro-PDEs, we then had a set of linear ODEs. At steady-state, this is a system of linear equations. We then solved for the binding rate that results in the experimentally measured steady-state ATPase by finding the null-space of a matrix). With saturating actin, the maximum steady-state ATPase rate is about 4s^{-1} [38], giving an attachment rate of $k_a = 6\text{s}^{-1}$. For both smooth and skeletal muscle, we assume a step of size $d = 10$nm [15]. Thus, the only parameter we cannot directly measure for smooth muscle is the cross-bridge stiffness k.

For skeletal muscle, ADP release is very fast at room temperature [31, 33], so we must estimate k_d^0 and δ_x indirectly (see the following section). Under the conditions considered here (ionic strength of about 0.025M and $T \approx 25$C), solution studies suggest that ATP binding occurs at about $k_t = 2\mu\text{M}^{-1}\text{s}^{-1}$ [33]. We use this value in our simulations. Steady-state ATPase is around 25s^{-1} [28, 4, 6, 7, 35]. With our parameters (some of which we estimate in the next section), a binding rate of $k_a = 40\text{s}^{-1}$ for skeletal muscle gives a similar

steady-state ATPase. Thus, there are three parameters we cannot directly measure for skeletal muscle: k_d^0, δ_x and k.

Determining k for smooth muscle

To estimate smooth muscle myosin's stiffness k, we used the motility measurements of Walcott et al. [53], Harris and Warshaw [16] and Harris and Warshaw [17] at $[ATP] = 1$mM. In these experiments, motility at 1mM ATP was between 0.5 and 0.7μm/s. Although some researchers report faster motility [e.g. 38], these lower values seem most consistent with the bulk of measurements in the literature [e.g. 46, 26]. We therefore performed a series of simulations allowing myosin's stiffness to vary, and determined what range of stiffnesses results in motility speeds between 0.5 and 0.7 μm/s.

We performed these simulations at variable myosin stiffness at $[ATP] = 1$mM using the Gillespie Algorithm. Complicating these simulations is the fact that we do not know the exact number of molecules interacting with an actin filament. We therefore considered ensembles of 100, 200 and 400 available myosin heads (there is little difference between these simulations). Comparing the model to experimental measurements, we find that k is between 0.22 - 0.32pN/nm (see Fig. 2a). Molecular stiffnesses larger than this value, say $k = 0.5$pN/nm strongly overestimate *in vitro* motility speed. Further supporting this stiffness estimate, we note that a molecular stiffness of $k = 0.3$pN/nm correctly predicts the actin filament length dependent motility experiments of Walcott et al. [53] and Harris and Warshaw [16], while higher molecular stiffnesses (e.g. $k = 0.5$pN/nm) are inconsistent with these data (see Fig. 2b). Thus, $k = 0.3$pN/nm is our best estimate of smooth muscle myosin's stiffness, although the actual stiffness may be as low as 0.22pN/nm or as high as 0.32pN/nm.

Determining k, δ_x and k_d^0 for skeletal muscle

For skeletal muscle, we must estimate k_d^0, δ_x and k. We assume that smooth and skeletal muscle myosin have similar stiffnesses, so that $k = 0.3$pN/nm. To find the remaining parameters (k_d^0 and δ_x), we used in vitro motility measurements at $[ATP] = 1$ mM [12] and a small ensemble force-velocity curve at $[ATP] = 100\mu$M [9]. We first performed a series of simulations of in vitro motility, systematically varying k_d^0 and δ_x to determine a range of parameters that are consistent with the measurements of Debold et al. [12]. We then performed simulations to determine which of these parameters (if any) were consistent with the small ensemble force-velocity measurements of Debold et al. [9]. Note that, based on the measurements of Marston and Taylor [31], we assume $k_d^0 \geq 350\text{s}^{-1}$.

For the motility assay, we used the Gillespie algorithm to simulate 100 available myosin heads at a series of solution ADP release rates from $k_d^0 = 300\text{s}^{-1}$ to $k_d^0 = 700\text{s}^{-1}$ ($k_d^0 = 300, 400, 500, 600$ and 700s^{-1}). At these ADP release rates, we varied the load dependent parameter δ_x from 0 to -2.0nm ($\delta_x = 0, -0.5, -1.0, -1.5$ and -2.0nm). The *in vitro* motility measurements of Debold et al. [12] are only consistent with a subset of these simulations (see Fig. 2c).

We chose parameters at the extreme of this subset, slow ADP release and large force-dependence ($k_d^0 = 350\text{s}^{-1}, \delta_x = -1.86$nm) and fast ADP release and small force-dependence ($k_d^0 = 650\text{s}^{-1}, \delta_x = 0$nm) to examine whether they were consistent with ensemble force-velocity data [9]. Simulations with fast ADP release and small force-dependence ($k_d^0 = 650\text{s}^{-1}, \delta_x = 0$nm) were inconsistent with the data, showing almost no curvature in the force-velocity relationship. However, simulations with slow ADP release and large force-dependence ($k_d^0 = 350\text{s}^{-1}, \delta_x = -1.86$nm) were consistent with the data (see Fig. 2d). We therefore chose this latter parameter set ($k_d^0 = 350\text{s}^{-1}, \delta_x = -1.86$nm) for our simulations.

Note that this parameter set successfully predicts single molecule measurements, in vitro motility at variable $[ATP]$, actin filament length-dependent in vitro motility and small ensemble force-velocity at $[ATP] = 30\mu$M (see Figs. 2, 3 and 4 of the main text). Thus, although we used a subset of experimental measurements to estimate parameters, the model successfully predicts a large number of measurements without doing any additional parameter fits. The model is therefore strongly supported by the data. Adding further support to the model is the observation that the fitting parameters are consistent with independent experimental measurements (see the section **In vitro mechanical data strongly support the model** in the main text).

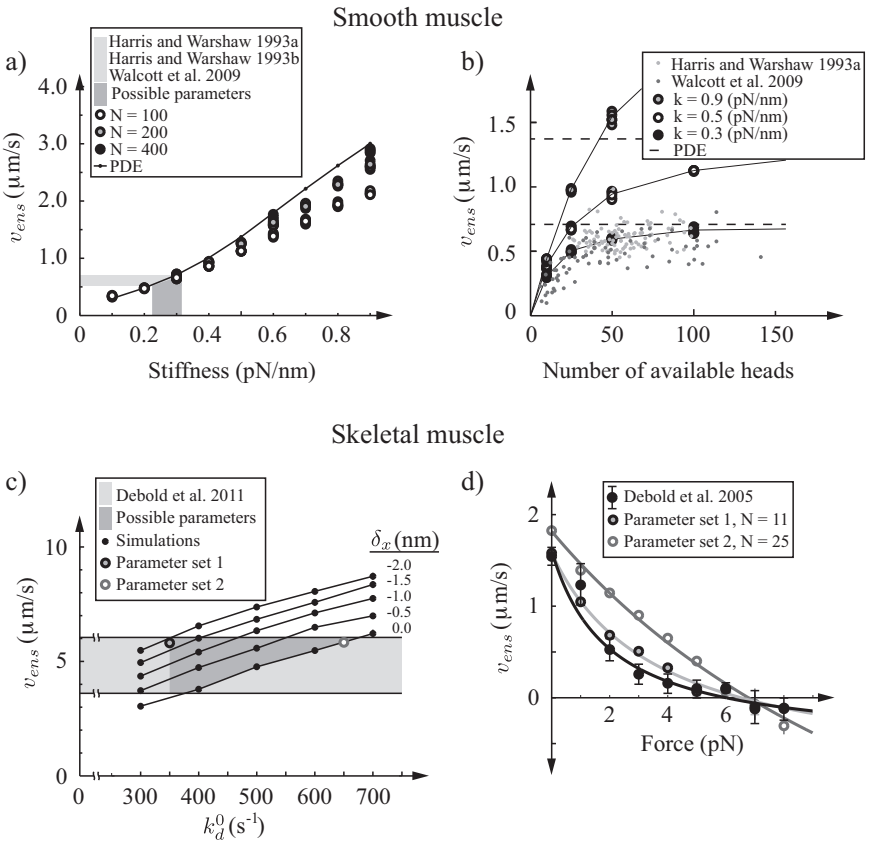

Figure 2: Estimating parameters in the model. a) Actin speed as a function of myosin stiffness for smooth muscle myosin for variable ensemble sizes. The range of experimental measurements is shown in light gray, the range of possible myosin stiffnesses in dark gray. The best fit value was $k = 0.3$pN/nm. b) Our estimate of myosin stiffness, $k = 0.3$pN/nm, also fits actin filament length dependent motility measurements. We show simulations for three values of myosin stiffness. Only $k = 0.3$ is consistent with experimental measurements. c) Actin speed as a function of unloaded ADP release rate, k_d^0, for several different force dependence values, δ_x. Only a subset of these simulations were consistent with the experimental measurements of Debold et al. [12] (the allowed parameters are shown in dark gray, experimental measurements in light gray). d) Only simulations with large force-dependent (δ_x) and small unloaded ADP release (k_d^0) are consistent with force-velocity measurements [9]. The best-fit values are $k_d^0 = 350\text{s}^{-1}$ and $\delta_x = -1.86$ (parameter set 1).

Simulation details

In order to best evaluate the model, we made an effort to simulate the physics of the experiments and to analyze the resulting simulated data using the same algorithms used to analyze experimental data. Here,

we describe the details of our simulation of each experimental system.

Single molecule laser trap

In the laser trap, an actin filament is manipulated via beads attached to either end. The lasers create a potential well that "traps" the beads. For small displacements, this potential is well-modeled as quadratic, though for large displacements non-linear terms must be taken into account. We assumed that the potential was precisely quadratic.

Brownian motion causes this bead-actin-bead assembly to fluctuate randomly. As the potential from the laser is approximately quadratic, the laser may be thought of as a linear spring with some stiffness k_{trap}. The position of the bead-actin-bead assembly therefore samples a Gaussian distribution with standard deviation proportional to the reciprocal of the square root of trap stiffness ($1/\sqrt{k_{trap}}$). Here, we have assumed Boltzmann statistics.

In general, we must consider the stiffness of the actin and the connection between the beads and actin. To model these effects, we would have to introduce additional parameters (the various stiffnesses) that are known only approximately [e.g. 50, 22, 27, 48]. In our model, for simplicity, we neglect these effects. We anticipate that this simplification will have only a small effect on our simulations, as various bead attachment procedures give similar results for step size and attachment time (e.g. biotin-avidin, NEM myosin [53, 15, 11]).

To collect data, the bead-actin-bead system (also called a "dumbbell") is moved toward a myosin molecule on the surface. The position of that myosin molecule fluctuates as a function of time due to Brownian motion. Again, assuming Boltzmann statistics, the molecule samples a Gaussian distribution of positions with standard deviation proportional to the square root of the reciprocal of myosin's stiffness ($1/\sqrt{k}$). Note that here, as with all simulations and experiments, "myosin's" stiffness includes both the stiffness of myosin itself, the stiffness of the protein used to attach myosin to the surface (if applicable) and the stiffness of the surface itself. These latter stiffnesses may or may not be negligible.

In our simulations, we used the Gillespie algorithm to determine when myosin initially binds to actin. At the initiation of binding, we determined where the dumbbell was with respect to the center of the laser's potential well (we picked a random number from a Gaussian distribution with standard deviation $\sqrt{k_BT/k_{trap}}$). We also determined where the myosin molecule was with respect to its undeformed position (we picked a random number from a Gaussian distribution with standard deviation $\sqrt{k_BT/k}$). We then assumed the system immediately came to mechanical equilibrium, but continued to fluctuate due to Brownian motion. Thus, since the stiffness of the dumbbell now included both the laser trap and myosin's stiffness, we assumed that the position of the dumbbell sampled a Gaussian distribution with standard deviation $\sqrt{k_BT/(k+k_{trap})}$.

Due to these thermal fluctuations of actin and myosin, a bound myosin molecule generally experiences non-zero average force. Specifically, since both the position of myosin and the position of the dumbbell fluctuate, when myosin binds to actin, neither is in its equilibrium position. Additionally, since a bound myosin rapidly undergoes its power stroke and the laser trap does not move, the laser trap applies an average non-zero force to myosin. This force affects myosin's ADP release rate. In our simulations, we determined the average force on myosin each time it bound to actin, and then used the average force to calculate the ADP release rate, which is in general not equal to the ADP release rate measured in solution k_d^0.

We assumed that the position was faithfully recorded by the quadrant photodiode (QPD), therefore neglecting electronic noise or other measurement noise. We sampled position at 4000 Hz, a similar rate to some experimental measurements [e.g. 1, 2, 53]. The resulting simulated data appeared similar to experimental measurements, although with a larger signal to noise ratio. This result is not surprising, as we neglect various sources of noise (e.g. actin-bead connection compliance, actin compliance, electronic noise, stage drift). We generated data traces over times comparable to experimental measurements.

We analyzed these data traces using mean-variance analysis [37, 15]. Our algorithm followed that described in Patlak [37]; our selection of the event population was similar to that used in experiments [e.g. 15]. Window widths were selected to be similar to experiments, and were varied to ensure that our simulation results remained the same for reasonable choices of these values. The simulated data appear similar to experimental measurements, though with less noise (compare Fig. 3 with Fig. 2 of Baker et al. [2]).

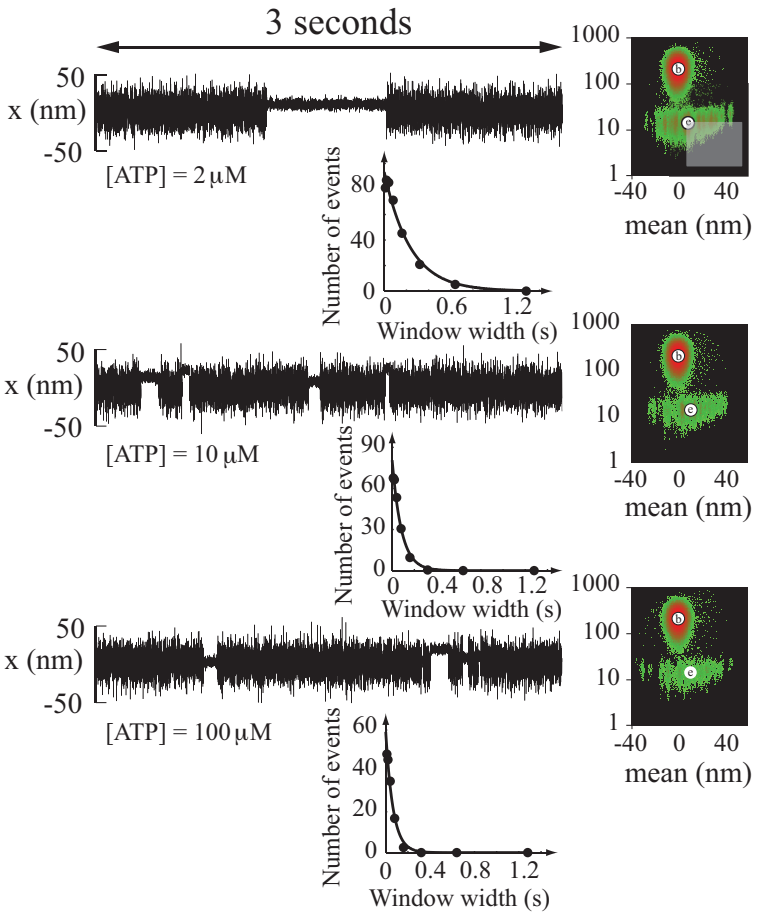

Figure 3: Simulated single molecule data. Three different ATP values are pictured, along with the Mean-Variance (MV) analysis [37, 15] of the traces (inset, right and below). The data used to find step size d_1 and attachment time t_1 is indicated in the top right MV histogram [15]. The simulated data are qualitatively similar to experimental measurements *cf* Fig. 2 of Baker et al. [2].

Small ensemble laser trap

In a laser trap experiment, if the surface density of myosin is sufficiently increased, the bead-actin-bead assembly (also called a dumbbell) moves smoothly over long distances. It is possible to program a computer to adjust laser position in real-time to apply a constant mean force on the dumbbell [9]. In a remarkable result, when the computer cycles through a ladder of forces and the mean velocity of the dumbbell is measured, the resulting force-velocity curve can be fit with the same curves that fit muscle fiber data [9, 18]. Note that this result occurs only for a narrow window of myosin surface densities: if the density is too low, smooth motion does not occur and force-velocity measurement becomes impossible; if the density is too high, it becomes impossible to apply sufficient force to slow the velocity of the dumbbell (the maximum force that can be applied to the system without breaking actin or pulling off the beads is around 15-20 pN).

Using the same physical model as in our single molecule laser trap simulations, we simulated these experiments. Since these simulations incorporate multiple myosin molecules, we had to calculate intermolecular forces. As before, we calculated the position of myosin and dumbbell position at the moment any new myosin attached. We assumed that mechanical equilibrium was achieved rapidly. Each myosin molecule therefore experienced (in general) a different non-zero force, and therefore had a different ADP release rate (following Bell's approximation). We readjusted dumbbell position upon detachment of myosin, and if all myosin detached, we repositioned the dumbbell back to a reference position (a similar procedure is used in

experiments).

To simulate varying the surface density of myosin, we varied the number of myosin molecules interacting with the dumbbell. We applied a constant force to the dumbbell, cycling through the same forces for the same times as were used in experiments [9, 53]. We then fit the data traces with linear curves, using the slopes of these curves as the average velocity (the same procedure was used in Debold et al. [9] and Walcott et al. [53]). Our simulated data was similar to experimental measurements (see Fig. 4 of the main paper).

As observed experimentally, in our simulations, these force-velocity measurements were only possible for a relatively narrow range of myosin surface densities. The data were best fit with densities near the lower bound. Note that, in experimental measurements, as the dumbbell is lowered to the surface, the probability of encountering a particular number of myosin molecules should have a Poisson distribution. Experiments are not a faithful representation of this distribution, but rather are skewed to favor successful measurements. For example, in one experiment, one might lower the dumbbell down to the surface several times before getting a data trace that can be analyzed. Presumably, some of these unusable data traces result from situations where too few myosin molecules interact with the dumbbell. Thus, the experimental data is biased towards the upper limit of the Poisson distribution.

In our simulations we neglect this complexity, assuming a constant number of myosin molecules interacting with the dumbbell. This simplifying assumption might explain why our error is smaller than experimental measurements [9, 53], as myosin number should vary in experiments. Additionally, this result might explain why we predict more myosin molecules interacting with actin than Debold et al. [9]. Specifically, they report the mean of the Poisson distribution, while we expect their measurements to be biased toward larger myosin numbers. The measurements of Walcott et al. [53] were at a higher density, and so we expect this bias to have a smaller effect.

It is worth noting that our model predicts that the force-velocity relationship measured in these small ensembles, though qualitatively similar to what would be measured in large ensembles, contains quantitative differences. In particular, large ensembles give force velocity curves that have higher curvature and faster unloaded speed (i.e. the data point at 0 force).

Motility assay

In an in vitro motility experiment, fluorescent actin filaments glide over a 2D surface covered with myosin. The 2D nature of this system is important in some experiments, particularly for long actin filaments at low myosin surface density [47]. However, at high myosin density or with relatively short filaments, the 2D nature should be less important since actin is stiff and is propelled unidirectionally. In our simulations, for simplicity we therefore assumed precisely 1D motility.

In each simulation, we simulated a constant number of myosin molecules interacting with an actin filament. We used the same basic simulation techniques as used in the small ensemble laser trap:

1. Using the Gillespie algorithm, determine which chemical reaction occurs and when that reaction happens;
2. Using a mechanical model of actin and myosin, determine their position upon attachment;
3. Keep track of the force on each myosin to determine individual ADP release rates;
4. Restore mechanical equilibrium upon the detachment or attachment of myosin;

If all myosin molecules detached, we assumed that (on average) actin remained stationary. Note that this assumption results in a slightly underestimated actin speed, since free actin should perform a random walk with non-zero speed. This effect is small.

To simulate filament length-dependent motility, we varied the number of myosin molecules interacting with a filament. We assume a constant number of myosin molecules, while experimentally, this number varies slightly.

Numerical simulation of integro-PDEs in steady state

We numerically simulated the integro-PDEs (Eqs. 1) at steady state and in the absence of external force (see Fig. 3 of the main text). A similar procedure can be used to simulate the integro-PDEs at variable force.

We start by assuming steady-state, which reduces the equations to a set of coupled integro-ODEs. We then choose to use mass conservation rather than the fourth equation of Eqs. 1:

$$\begin{aligned} v\frac{d\eta_2}{dx} &= \kappa_a(x)n_1 - k_d(x)\eta_2 \\ v\frac{d\eta_3}{dx} &= k_d(x)\eta_2 - k_T[T]\eta_3 \\ 0 &= k_T[T]\int_{-\infty}^{\infty}\eta_3 dx + n_1 k_h^- - n_4 k_h^+ \\ 1 &= n_1 + n_4 + \int_{-\infty}^{\infty}\eta_2 dx + \int_{-\infty}^{\infty}\eta_3 dx \end{aligned} \tag{13}$$

We then have the constraint that the overall force is zero:

$$\int_{-\infty}^{\infty} k(x+d)\eta_2 dx + \int_{-\infty}^{\infty} k(x+d)\eta_3 dx = 0$$

Given values for v, $\int_{-\infty}^{\infty}\eta_2 dx$ and $\int_{-\infty}^{\infty}\eta_3 dx$, we could solve these equations. We therefore assume a value of v and perform a root find (e.g. Newton's method) to find the values of $\int_{-\infty}^{\infty}\eta_2 dx$ and $\int_{-\infty}^{\infty}\eta_3 dx$ that satisfy conservation of mass. In general, the value of v we pick will not satisfy the zero force constraint, so we must do another root find on v to satisfy this constraint. We therefore have two nested root finds, which is computationally expensive. We may nevertheless perform these numerical simulations at variable concentrations of ATP (see Fig. 3 of the main text). To generate a force-velocity curve, we would simply use a non-zero force constraint. These numerical simulations allow us to determine myosin's behavior in the limit of an infinitely large ensemble.

Data selection

Many different labs have performed mechanical experiments on actin and myosin in vitro at both the single molecule and ensemble level. There are some inconsistencies in these measurements. For example, myosin's unitary step size has been reported to be 5 nm [32], 10 nm [15, 14], 8 nm [25] and more than 20 nm [43]. Some of these discrepancies may be due to different myosin preparations, with the S1 fragment tending to produce smaller unitary steps than heavy meromyosin (HMM) or intact myosin [23]. Alternatively, differences may arise due to data analysis methods. It is not our aim to resolve these discrepancies; instead, we wish to address discrepancies between single molecule and ensemble experiments from the same lab under similar conditions [e.g. 1, 2]. As small ensemble force-velocity measurements have been performed only by a single lab (the Warshaw lab [9, 10, 53]), we have selected measurements primarily from this group. In this way, we have tried to control, as much as possible, effects due to different experimental conditions, preparations, buffers or more subtle variations.

Do we neglect important effects?

To keep the model simple, we have neglected some aspects of the interaction of actin and myosin. That the model fits experimental data justifies our assumptions to some degree. Nevertheless, these neglected effects might have an impact on our parameter estimates. We therefore now briefly discuss two effects that we neglect in our model: first, the sub-step that occurs upon ADP release, and second actin compliance.

How does a sub step upon ADP release change the model?

There is experimental evidence to suggest that myosin does not perform its entire power stroke at once [49, 5]. In particular, upon strong binding, myosin is thought to undergo the majority of its power stroke, but the remaining few nanometers of displacement occurs during ADP release. Indeed, it is this small displacement upon ADP release that underlies its force-dependence [e.g. 49, 24]. In our model, we neglect this sub-step since it adds another difficult-to-measure parameter to the model. We nevertheless retain the

force-dependence of ADP release, so our assumption is the sub-step is small compared to the step that occurs upon the initiation of strong binding. Here, we argue that our assumption has only a small effect on our parameter estimates.

To understand how neglecting the sub-step affects our model, consider the analytic calculation of actin velocity from Eq. 8. This calculation remains the same regardless of the existence of a sub-step. In the calculation, we found that the non-dimensional speed $\mathcal{V}$ depends only on the variable $E = -k\delta_x d/k_B T$. Here, d is the displacement that occurs upon the initiation of strong binding. For smooth muscle, assuming that $d = 10$nm, we estimated that $E \approx 1.88$ from fits to experimental data, which since $\delta_x = -2.6$nm, gives an estimate for myosin stiffness $k = 0.3$pN/nm.

Now, suppose that there is a 3 nm sub-step that occurs upon ADP release, so the actual value of d is 7 nm. We then find that $k = -Ek_BT/\delta_x d = (1.88)(4.14\text{pN}\cdot\text{nm})/(2.6\text{nm})(7\text{nm}) = 0.43$pN/nm. This value is similar to our estimate of $k = 0.3$pN/nm and both are within the experimental error of the measurements of Veigel et al. [48]. Being within the bounds of experimental error, we argue that this error of a few tenths of a pN/nm is, for our purposes, negligible. Note that this effect is most pronounced in smooth muscle, where the sub-step is thought to be larger than in skeletal [49, 5].

How does actin elasticity change the model?

We assume that actin is perfectly rigid. Recent simulations have argued that actin elasticity is important and, at least for some applications, should not be neglected [44]. Additionally, at low myosin density, long actin filaments are thought to bend, leading to slower motility than would be predicted with rigid filaments [47]. Here, we argue that for the experimental conditions considered here, rigid actin is a reasonable assumption. We then briefly discuss how actin compliance would qualitatively affect our results.

Assuming actin acts as a thin, linearly elastic, cylindrical beam subject to locally small deformations, we can relate its persistence length to its stiffness. In particular, actin's persistence length L_p has been measured to be between 10 and 20 μm [34]. Using the relationship $L_p = E_m I/k_B T$, where I is the second moment of area and E_m is the Young's modulus, and assuming a radius of 5nm for actin, actin's Young's modulus is $E_m \approx 100$MPa. For two myosin molecules 100nm apart (the lowest density of myosin we consider, see Table 2 of the main text), the stiffness of the intervening actin is $k_{actin} = EA/L \approx 80$pN/nm. Comparing this value to myosin's stiffness, $k = 0.3$pN/nm, it is clear that myosin's compliance dominates actin's compliance. For example, if each myosin of the two myosin molecules 100 nm apart generate 4 pN of force, the myosin molecules would deform 13 nm, while actin would deform half an Angstrom.

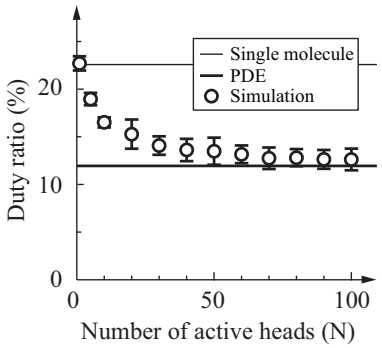

Figure 4: Duty ratio varies with ensemble size. Monte-Carlo simulations of smooth muscle myosin at 1mM ATP demonstrate that duty ratio decreases as ensemble size increases. Note that here we consider duty ratio per active myosin head. If only one of myosin's two heads is active [45, 23, 52], duty ratio per head [e.g. 16] is half this value.

We can qualitatively understand how actin compliance would affect our results. Specifically, from the analytic calculation of actin velocity from Eq. 8, we know that actin speed depends only on the parameter $E = -k\delta_x d/k_B T$. This parameter determines how much previously attached myosin molecules are deformed when an additional myosin molecule binds and undergoes its power stroke (see the **Discussion** of the

main text). Decreasing the stiffness of actin lowers the effective stiffness k, lowers E, and therefore decreases intermolecular interactions. Thus, increasing actin compliance would decrease, but not eliminate, the myosin-induced changes in attachment time, attachment distance and actin speed.

Finally, we note that actin deformation may change myosin's ability to bind, unbind or undergo molecular transitions. Such effects may occur, but we did not need to incorporate them into our model in order to fit the data. Thus, our assumption of actin's rigidity is justified for the experimental conditions considered here.

A demonstration that myosin's duty ratio varies with ensemble size

Uyeda et al. [47] introduced a simple method to estimate myosin's duty ratio at a given ATP concentration and in the absence of force. This technique was modified by [16], and remains a useful tool [53]. This method implicitly assumes that myosin's duty ratio is constant and independent of ensemble size. Our model provides evidence that myosin's strong binding lifetime varies with ensemble size, raising the possibility that duty ratio varies with ensemble size. We performed a series of simulations explicitly demonstrating this effect (see Fig. 4). In the simulations of smooth muscle myosin, duty ratio drops by a factor of two as ensemble size increases.

A demonstration that attachment rate affects detachment-limited motility speed

Detachment limited motility describes actin speed that is limited by myosin's unbinding from actin. Under these conditions, one may write actin's speed as [40, 21]

$$v_{act} = \frac{d_{on}}{t_{on}}$$

where t_{on} is the expected lifetime of strong binding and d_{on} is the expected distance that actin moves relative to myosin during this strong binding. In order for this expression to be correct, there must always be at least one myosin interacting with actin at any given time. Strictly, this condition holds only when there are an infinite number of myosin molecules that may bind to actin; practically, this condition is approximately correct even for relatively small ensembles (our simulations suggest only a 10% error for ensembles of 20 or 30 available heads, see Fig. 5a).

Our model demonstrates that d_{on} and t_{on} vary as a function of ensemble size (see Fig. 5c). This result raises the possibility that, even when motility is detachment limited (as defined above), increasing myosin's attachment rate to myosin (k_a) can increase motility rate. We performed a series of simulations that demonstrate this effect.

Let us suppose that we have an ensemble of smooth muscle myosin that undergoes the kinetic scheme in Fig. 1 with parameters as described in Table 1 of the main text. Further, let us suppose that we can measure d_{on} and t_{on} and v_{act} independently (see Fig. 5c). There will be some error associated with our measurements, so let's assume that if v_{act} is within 10% of d_{on}/t_{on}, then motility is detachment limited (i.e. detachment limited motility occurs if $(d_{on}/t_{on} - v_{act})/v_{act} < 10\%$). This 10% cutoff is arbitrary, the following demonstration works for any constant percent error.

Given these assumptions, we find that at 1mM ATP, 20-30 myosin molecules result in detachment limited motility. However, if we increase ensemble size, we can increase v_{act} from 0.5μm/s to 0.7μm/s an increase of 40% – well beyond the sensitivity of our measurement (see Fig 5a). Therefore, if we increase attachment rate we can get a measurable increase in v_{act}. We explicitly demonstrate this effect in Figure 5b, where we consider an ensemble of 50 myosin molecules. Thus, although motility is detachment limited to within experimental resolution, attachment rate affects motility speed (v_{act}).

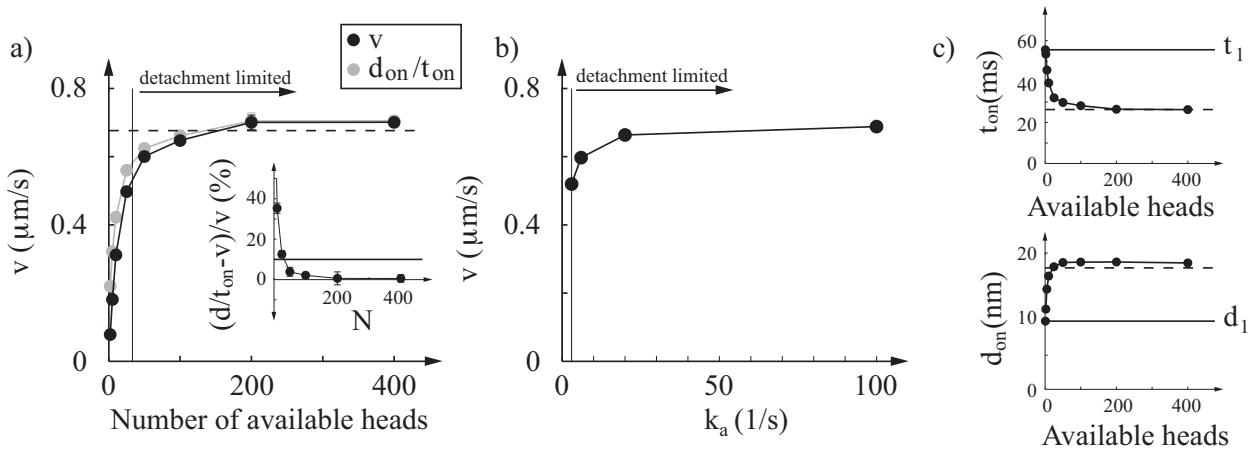

Figure 5: Simulations of smooth muscle myosin at $[ATP] = 1\text{mM}$, demonstrating attachment rate affecting detachment limited motility speed. a) Motility speed (black) and attachment distance d_{on} divided by attachment time t_{on} (gray) as a function of the number of available myosin heads. When the two measurements are within 10% motility is detachment limited. Inset shows the percent difference, with a solid line at 10%. For reference, the simple approximation of Eq. 8 is shown as a black dashed line. b) Motility speed as a function of attachment rate for an ensemble of 50 available heads. Motility speed increases by about 40%. c) Attachment time t_{on} and attachment distance d_{on} as a function of ensemble size. For reference, the simple approximations of Eq. 10 and 12 are shown (black dashed lines), as are the single molecule measurements t_1 and d_1 (black solid lines).

References

[1] J. E. Baker, C. Brosseau, P. B. Joel, and D. M. Warshaw. The biochemical kinetics underlying actin movement generated by one and many skeletal muscle myosin molecules. *Biophysical Journal*, 82: 2134–2147, 2002.

[2] J. E. Baker, C. Brosseau, P. Fagnant, and D. M. Warshaw. The unique properties of tonic smooth muscle emerge from intrinsic as well as intermolecular behaviors of myosin molecules. *Journal of Biological Chemistry*, 278:28533–28539, 2003.

[3] G. I. Bell. Models for the specific adhesion of cells to cells. *Science*, 200:618–627, 1978.

[4] M. Brune, J. L. Hunter, J. E. T. Corrie, and M. R. Webb. Direct, real-time measurement of rapid inorganic phosphate release using a novel fluorescent probe and its application to actomyosin sub fragment 1 ATPase. *Biochemistry*, 33:8262–8271, 1994.

[5] M. Capitanio, M. Canepari, P. Cacciafesta, V. Lombardi, R. Cicchi, M. Maffei, F. S. Pavone, and R. Bottinelli. Two independent mechanical events in the interaction cycle of skeletal muscle myosin with actin. *Proceedings of the National Academy of Sciences*, 103:87–92, 2006.

[6] J. Chalovich and E. Eisenberg. Inhibition of actomyosin ATPare activity by troponin-tropomyosin without blocking the binding of myosin to actin. *Journal of Biological Chemistry*, 257:2432–2437, 1982.

[7] J. Chalovich and E. Eisenberg. The effect of troponin-tropomyosin on the binding of heavy meromyosin to actin in the presence of ATP. *Journal of Biological Chemistry*, 261:5088–5093, 1982.

[8] C. R. Cremo and M. A. Geeves. Interaction of actin and ADP with the head domain of smooth muscle myosin: implications for strain-dependent ADP release in smooth muscle. *Biochemistry*, 37:1969–1978, 1998.

[9] E. P. Debold, J. B. Patlak, and D. M. Warshaw. Slip sliding away: load-dependence of velocity generated by skeletal muscle myosin molecules in the laser trap. *Biophysical Journal*, 89:L34–L36, 2005.

[10] E. P. Debold, J. P. Schmitt, J. B. Patlak, S. E. Beck, J. R. Moore, J. G. Seidman, C. Seidman, and D. M. Warshaw. Hypertrophic and dilated cardiomyopathy mutations differentially affect the molecular force generation of mouse α-cardiac myosin in the laser trap assay. *American Journal of Physiology*, 293:H284–H291, 2007.

[11] E. P. Debold, S. E. Beck, and D. M. Warshaw. Effect of low pH on single skeletal muscle myosin mechanics and kinetics. *American Journal of Physiology*, 295:C173–C179, 2008.

[12] E. P. Debold, M. Turner, J. C. Stout, and S. Walcott. Phosphate enhances myosin-powered actin filament velocity under acidic conditions in a motility assay. *American Journal of Physiology*, 300: R1401–R1408, 2011.

[13] T. A. J. Duke. Molecular model of muscle contraction. *PNAS*, 96:2770–2775, 1999.

[14] J. T. Finer, R. M. Simmons, and J. A. Spudich. Single myosin molecule mechanics: piconewton forces and nanometre steps. *Nature*, 368:113–119, 1994.

[15] W. H. Guilford, D. E. Depuis, G. Kennedy, J. Wu, J. B. Patlak, and D. M. Warshaw. Smooth muscle and skeletal muscle myosin produce similar unitary forces and displacements in the laser trap. *Biophysical Journal*, 72:1006–1021, 1997.

[16] D. E. Harris and D. M. Warshaw. Smooth and skeletal muscle myosin both exhibit low duty cycles at zero load in vitro. *Journal of Biological Chemistry*, 268:14764–14768, 1993.

[17] D. E. Harris and D. M. Warshaw. Smooth and skeletal muscle actin are mechanically indistinguishable in the in vitro motility assay. *Circulation Research*, 72:219–224, 1993.

[18] A. V. Hill. The heat of shortening and the dynamic constants of muscle. *Proceedings of the Royal Society of London. Series B, Biological Sciences*, 126:136–195, 1938.

[19] J. Howard. *Mechanics of motor proteins and the cytoskeleton*. Sinauer Associates, 2001.

[20] A. F. Huxley. Muscle structure and theories of contraction. *Progress in Biophysics and Biophysical Chemistry*, 7:255–318, 1957.

[21] H. E. Huxley. Sliding filaments and molecular motile systems. *Journal of Biological Chemistry*, 265: 8347–8350, 1990.

[22] H. E. Huxley, A. Stewart, H. Sosa, and T. Irving. X-ray diffraction measurements of the extensibility of actin and myosin filaments in contracting muscle. *Biophysical Journal*, 67:2411–2421, 1994.

[23] N. M. Kad, A. S. Rovner, P. M. Fagnant, P. B. Joel, G. G. Kennedy, J. B. Patlak, D. M. Warshaw, and K. M. Trybus. A mutant heterodimeric myosin with one inactive head generates maximal displacement. *Journal of Cell Biology*, 162:481–488, 2003.

[24] N. M. Kad, J. B. Patlak, P. M. Fagnant, K. M. Trybus, and D. M. Warshaw. Mutation of a conserved glycine in the SH1-SH2 helix affects the load-dependent kinetics of myosin. *Biophysical Journal*, 92: 1623–1631, 2007.

[25] M. Kaya and H. Higuchi. Nonlinear elasticity and an 8-nm working stroke of single myosin molecules in myofilaments. *Science*, 329:686–689, 2010.

[26] C. A. Kelley, M. Takahashi, J. H. Yu, and R. S. Adelstein. An insert of seven amino acids confers functional differences between smooth muscle myosins from the intestines and vasculature. *Journal of Biological Chemistry*, 268:12848–12854, 1993.

[27] H. Kojima, A. Ishijima, and T. Yanagida. Direct measurement of stiffness of single actin filaments with and without tropomyosin by in vitro nanomanipulation. *Proceedings of the National Academy of Sciences*, 91:12962–12966, 1994.

[28] M. Kovacs, J. Tóth, C. Hetényi, A. Málnási-Csizmadia, and J. R. Sellers. Mechanism of blebbistatin inhibition of myosin II. *Journal of Biological Chemistry*, 279:35557–35563, 2004.

[29] H. M. Lacker. *Cross-bridge dynamics in skeletal muscle: mathematical methods for determining the reaction rate and force-extension curves of cross-bridges from the macroscopic behavior of muscle.* PhD thesis, New York University, 1977.

[30] H. M. Lacker and C. S. Peskin. A mathematical method for the unique determination of cross-bridge properties from steady-state mechanical and energetic experiments on macroscopic muscle. *Lectures on mathematics in the life sciences*, 16:121–153, 1986.

[31] S. B. Marston and E. W. Taylor. Comparison of the myosin and actomyosin ATPase mechanisms of the four types of vertebrate muscles. *Journal of Molecular Biology*, 139:573–600, 1980.

[32] J. E. Molloy, J. E. Burns, J. C. Sparrow, R. T. Tregear, J. Kendrick-Jones, and D. C. White. Single-molecule mechanics of heavy meromyosin and S1 interacting with rabbit or Drosophila actins using optical tweezers. *Biophysical Journal*, 68:298S–305S, 1995.

[33] M. Nyitrai, R. Rossi, N. Adamek, M. A. Pellegrino, R. Bottinelli, and M. A. Geeves. What limits the velocity of fast-skeletal muscle contraction in mammals? *Journal of Molecular Biology*, 355:432–442, 2006.

[34] A. Ott, M. Magnasco, A. Simon, and A Libchaber. Measurement of the persistence length of polymerized actin using fluorescence microscopy. *Physical Review E*, 48:R1642–R1645, 1993.

[35] S. C. Pastra-Landis, T. Huiatt, and S. Lowey. Assembly and kinetic properties of myosin light chain isozymes from fast skeletal muscle. *Journal of Molecular Biology*, 170:403–422, 1983.

[36] E. Pate and R. Cooke. A model of crossbridge action: the effects of ATP, ADP and Pi. *Journal of Muscle Research and Cell Motility*, 10:181–196, 1989.

[37] J. B. Patlak. Measuring kinetics of complex single ion channel data using mean-variance histograms. *Biophysical Journal*, 65:29–42, 1993.

[38] A. S. Rovner, P. M. Fagnant, and K. M. Trybus. Phosphorylation of a single head of smooth muscle myosin activates the whole molecule. *Biochemistry*, 45:5280–5289, 2006.

[39] J. R. Sellers, E. Eisenberg, and R. S. Adelstein. The binding of smooth muscle heavy meromyosin to actin in the presence of atp. *Journal of Biological Chemistry*, 257:13880–13883, 1982.

[40] R. F. Siemankowski, M. O. Wiseman, and H. D. White. Adp dissociated from actomyosin sub fragment-1 is sufficiently slow to limit the unloaded shortening velocity in vertebrate muscle. *Proceedings of the National Academy of Sciences*, 82:658–662, 1985.

[41] M. Srinivasan and S. Walcott. Binding site models of friction due to the formation and rupture of bonds: state-function formalism, force-velocity relations, response to slip velocity transients and slip stability. *Physical Reviews E*, 80:046124, 2009.

[42] H. L. Sweeney, S. S. Rosenfeld, F. Brown, L. Faust, J. Smith, J. Xing, L. A. Stein, and J. R. Sellers. Kinetic tuning of myosin via a flexible loop adjacent to the nucleotide binding pocket. *Journal of Biological Chemistry*, 273:6262–6270, 1998.

[43] H. Tanaka, K. Homma, H. D. White, T. Yanagida, and M. Ikebe. Smooth muscle myosin phosphorylated at single head shows sustained mechanical activity. *Journal of Biological Chemistry*, 283:15611–15618, 2008.

[44] B. C. W. Tanner, T. L. Daniel, and M. Regnier. Sarcomere lattice geometry influences cooperative myosin binding in muscle. *PLoS Computational Biology*, 3:e115, 2007.

[45] M. J. Tyska, D. E. Dupuis, W. H. Guilford, J. B. Patlak, G. S. Waller, K. M. Trybus, D. M. Warshaw, and S. Lowey. Two heads of myosin are better than one for generating force and motion. *Proceedings of the National Academy of Sciences*, 96:4402–4407, 1999.

[46] S. Umemoto and J. R. Sellers. Characterization of in vitro motility assays using smooth muscle and cytoplasmic myosins. *Journal of Biological Chemistry*, 265:14864–14869, 1990.

[47] T. Q. P. Uyeda, S. J. Kron, and J. A. Spudich. Myosin step size: estimation from slow sliding movement of actin over low densities of heavy meromyosin. *Journal of Molecular Biology*, 214:699–710, 1990.

[48] C. Veigel, M. L. Bartoo, D. C. S. White, J. C. Sparrow, and J. E. Molloy. The stiffness of rabbit skeletal actomyosin cross-bridges determined with an optical tweezers transducer. *Biophysical Journal*, 75:1424–1438, 1998.

[49] C. Veigel, J. E. Molloy, S. Schmitz, and J. Kendrick-Jones. Load-dependent kinetics of force production by smooth muscle myosin measured with optical tweezers. *Nature Cell Biology*, 5:980–986, 2003.

[50] K. Wakabayashi, Y. Sugimoto, H. Tanaka, Y. Ueno, Y. Takezawa, and Y. Amemiya. X-ray diffraction evidence for the extensibility of actin and myosin filaments during muscle contraction. *Biophysical Journal*, 67:2422–2435, 1994.

[51] S. Walcott and S. X. Sun. Hysteresis in cross-bridge models of muscle. *Physical Chemistry Chemical Physics*, 11:4871–4881, 2009.

[52] S. Walcott and D. M. Warshaw. Modeling smooth muscle myosin's two heads: long-lived enzymatic roles and phosphorylation-dependent equilibria. *Biophysical Journal*, 99:1129–1138, 2010.

[53] S. Walcott, P. M. Fagnant, K. M. Trybus, and D. M. Warshaw. Smooth muscle heavy meromyosin phosphorylated on one of its two heads supports force and motion. *Journal of Biological Chemistry*, 284:18244–18251, 2009.

[54] D. M. Warshaw. The in vitro motility assay: a window into the myosin molecular motor. *News in Physiological Sciences*, 11:1–7, 1996.